IOP Publishing | Institute of Physics and Engineering in Medicine Physics in Medicine & Biology

Phys. Med. Biol. **60** (2015) 3747–3757 doi:10.1088/0031-9155/60/9/3747

Acousto-electrical speckle pattern in Lorentz force electrical impedance tomography

Pol Grasland-Mongrain[1], François Destrempes[1], Jean-Martial Mari[2], Rémi Souchon[3,4], Stefan Catheline[3,4], Jean-Yves Chapelon[3,4], Cyril Lafon[3,4] and Guy Cloutier[1,5]

[1] Laboratoire de Biorhéologie et d'Ultrasonographie Médicale, Centre Hospitalier de l'Université de Montréal (CRCHUM), Tour Viger, 900 rue Saint-Denis, Montréal (QC) H2X 0A9, Canada
[2] GePaSud, University of French Polynesia, Polynésie Française
[3] Inserm, U1032, LabTau, Lyon F-69003, France
[4] Université de Lyon, Lyon F-69003, France
[5] Département de radiologie, radio-oncologie et médecine nucléaire, et Institut de génie biomédical, Université de Montréal, Montréal (QC) H3T 1J4, Canada

E-mail: pol.grasland-mongrain@ens-cachan.org and guy.cloutier@umontreal.ca

Received 29 September 2014, revised 24 February 2015
Accepted for publication 31 March 2015
Published 23 April 2015

Abstract

Ultrasound speckle is a granular texture pattern appearing in ultrasound imaging. It can be used to distinguish tissues and identify pathologies. Lorentz force electrical impedance tomography is an ultrasound-based medical imaging technique of the tissue electrical conductivity. It is based on the application of an ultrasound wave in a medium placed in a magnetic field and on the measurement of the induced electric current due to Lorentz force. Similarly to ultrasound imaging, we hypothesized that a speckle could be observed with Lorentz force electrical impedance tomography imaging. In this study, we first assessed the theoretical similarity between the measured signals in Lorentz force electrical impedance tomography and in ultrasound imaging modalities. We then compared experimentally the signal measured in both methods using an acoustic and electrical impedance interface. Finally, a bovine muscle sample was imaged using the two methods. Similar speckle patterns were observed. This indicates the existence of an 'acousto-electrical speckle' in the Lorentz force electrical impedance tomography with spatial characteristics driven by the acoustic parameters but due to electrical impedance inhomogeneities instead of acoustic ones as is the case of ultrasound imaging.

Keywords: Lorentz force, electrical impedance tomography, magneto-acousto-electrical tomography, electrical conductivity, speckle

(Some figures may appear in colour only in the online journal)

1. Introduction

Ultrasound (US) B-mode is a widespread medical imaging technique of the tissue acoustical impedance. With this technique, an ultrasound wave is transmitted by an acoustic transducer and is backscattered by the change in acoustic impedance at tissue interfaces. Measuring the analytic signal obtained from ultrasound waves received on the transducer surface leads to the reconstruction of these acoustic impedance interfaces. Moreover, when ultrasound waves are scattered by acoustic impedance inhomogeneities, their contributions add up constructively or destructively on the transducer surface. The total intensity thus varies randomly due to these interferences (Cobbold 2007). The phenomenon appears on reconstructed images as a granular pattern with variable size and intensity, which looks spatially random: it is called 'acoustic speckle' (Abbott and Thurstone 1979).

The speckle can be treated as noise and consequently be reduced, or on the contrary be considered as a feature (Noble and Boukerroui 2006). Under the first point of view, quantitative ultrasound methods were proposed based on the backscattering coefficient (Lizzi *et al* 1983, Lizzi *et al* 1987, Insana *et al* 1990), where the speckle is removed to obtain a measure that depends only on tissue acoustic properties; see Goshal *et al* (2013) for further references. Under the second point of view, quantitative ultrasound methods were developed by exploiting the statistics of the echo envelope (Burckhardt 1978, Wagner *et al* 1983) that depend on the speckle and tissue characteristics to discriminate tissue types; see Destrempes and Cloutier (2010, 2013) and Yamaguchi (2013) for further references. In either case, quantitative ultrasound can be used to diagnose pathologies with ultrasound images. Another field of application is speckle-tracking that aims at estimating local displacements and tissue deformations; see for instance (Ophir *et al* 1991, Hein and O'Brien 1993, Lubinski *et al* 1999).

On the other hand, the Lorentz force electrical impedance tomography (LFEIT) method (Montalibet 2001, Grasland-Mongrain *et al* 2013), also known as magneto-acousto electrical tomography (Haider *et al* 2008), is a medical imaging technique producing electrical conductivity images of tissues (Roth *et al* 1994, Wen *et al* 1998, Ammari *et al* 2014). With this technique, an ultrasound wave is transmitted by an acoustic transducer in a biological tissue placed in a magnetic field. The movement of the tissue in the magnetic field due to the ultrasound propagation induces an electric current due to Lorentz force. The measurement of this current with electrodes in contact with the sample allows to reconstruct images of electrical impedance interfaces.

The goal of this work was to assess the presence of an 'acousto-electrical' speckle in the LFEIT technique, similar to the acoustic speckle in US imaging, as suggested in a previous work (Haider *et al* 2008). The first part of this work presents the theoretical similarity of measured signals in these two imaging techniques. This similarity is then observed experimentally on an acoustic and electrical interface. Finally, a bovine sample is imaged using both methods to observe the two types of speckle.

2. Theoretical background

The goal of this section is to compare the mathematical framework of the LFEIT method with that describing radio-frequency signals in US imaging.

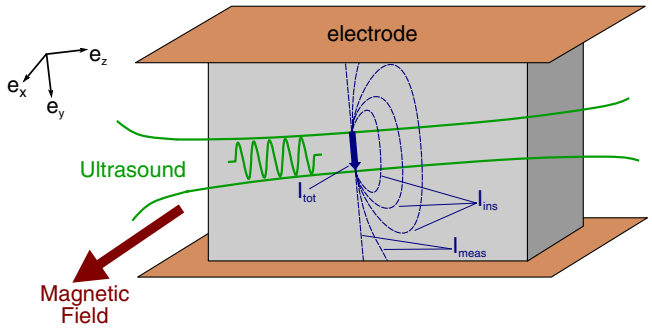

Figure 1. An ultrasound wave is transmitted in a conductive medium placed in a magnetic field. This induces an electric current I_{tot} due to Lorentz force. This current separates in two components, I_{ins} which stays inside the medium, and I_{meas} which is measured by electrodes in contact. The measured signal allows one to reconstruct images of electrical impedance interfaces.

2.1. Local current density in Lorentz force electrical impedance tomography

The LFEIT principle is illustrated in figure 1. In this technique, an ultrasound wave is transmitted along a unit vector $\mathbf{e}_z$ in a conductive medium placed in a magnetic field along $\mathbf{e}_x$ of intensity B_x. This induces an electric current due to Lorentz force in the direction $\mathbf{e}_y = \mathbf{e}_z \times \mathbf{e}_x$. We assume that the conductive medium is moved by the ultrasound wave along the $\mathbf{e}_z$ direction so that all particles within the medium are moved with a mean velocity of amplitude v_z parallel to $\mathbf{e}_z$ (Mari *et al* 2009). Since the medium is placed in a magnetic field B_x, a particle k of charge q_k is deviated by a Lorentz force $\mathbf{F}_k = q_k v_z B_x \, \mathbf{e}_y$. Using Newton's second law, the velocity $\mathbf{u}_k$ of the charged particle can be calculated as:

$$\mathbf{u}_k = v_z \mathbf{e}_z + \mu_k v_z B_x \mathbf{e}_y, \tag{1}$$

where μ_k is the mobility of the particle k.

The density of current $\mathbf{j}$, defined as $\sum_k q_k \, \mathbf{u}_k$ per unit volume, is then equal to the sum of $\sum_k q_k v_z \mathbf{e}_z$ and $\sum_k q_k \mu_k v_z B_x \mathbf{e}_y$ per unit volume. If the medium is assumed electrically neutral, i.e. $\sum_k q_k = 0$, the first term is equal to zero. By introducing the electrical conductivity σ, defined as $\sum_k q_k \mu_k$ per unit volume, the second term is equal to $\sigma \, v_z B_x \, \mathbf{e}_y$. Equation (1) can consequently be written as:

$$\mathbf{j} = \sigma v_z B_x \mathbf{e}_y. \tag{2}$$

The local density of current $\mathbf{j}$ is thus proportional to the electrical conductivity of the sample σ, to the component B_x of the applied magnetic field, and to the local sample speed v (Montalibet 2001).

2.2. Measured signal in Lorentz force electrical impedance tomography

Equation (2) is however local. We consider, as a first approximation, the ultrasound beam as a plane wave along $\mathbf{e}_z$ inside a disk of diameter W, with the velocity $v_z = 0$ outside the beam. The total current I_{tot} induced by the Lorentz force is then equal to the average of the current density j computed over all surfaces S inside the ultrasound beam that are perpendicular to e_y (Montalibet *et al* 2002):

$$I_{\text{tot}}(t) = \frac{1}{W} \iiint \mathbf{j}.\mathbf{dS} \, \mathrm{d}y = \frac{1}{W} \iiint \sigma v_z B_x \, \mathrm{d}z \, \mathrm{d}x \, \mathrm{d}y. \tag{3}$$

As electrodes are placed outside the beam, we assume they measure only a fraction α of the total current I_{tot} induced by the Lorentz force. The current I_{tot} then induces a current outside the beam which separates in two components: a current I_{ins} that stays inside the medium and operates through a resistance R_{ins}, and a current I_{meas} that is measured by electrodes and operates through a resistance R_{meas}. Due to Ohm's law, which states that $I_{ins}R_{ins} = I_{meas}R_{meas}$, the coefficient α, defined as I_{meas}/I_{tot}, is also equal to $R_{ins}/(R_{meas} + R_{ins})$. This coefficient, rather difficult to estimate, depends consequently on a few parameters: the size and location of electrodes, and the circuit and medium electrical impedance. We can nevertheless conclude that the lower the resistance R_{meas} compared to R_{ins}, the higher α is, and the higher is the measured electrical current.

For a linear and inviscid medium, the medium velocity v_z due to ultrasound wave propagation is related to the ultrasound pressure p and the medium density ρ (assumed here constant over time but not necessarily over space) using the identity $\frac{\partial v_z(t,z)}{\partial t} = -\frac{1}{\rho}\frac{\partial p(t,z)}{\partial z}$ (having assumed a plane wave). From these considerations on the coefficient α and the medium velocity v_z, the measured current I_{meas} is equal to:

$$I_{meas}(t) = \frac{\alpha}{W}\int\int\int_{z_1}^{z_2} \sigma B_x \left(\int_{-\infty}^{t} -\frac{1}{\rho}\frac{\partial p(\tau, z)}{\partial z}\, \mathrm{d}\tau \right) \mathrm{d}z\ \mathrm{d}x\ \mathrm{d}y, \tag{4}$$

where z_1 and z_2 are the boundaries of the studied medium along $\mathbf{e}_z$.

Considering a progressive acoustic wave that propagates only along the direction $\mathbf{e}_z$ and is not attenuated in the measurement volume, we may assume that $p(\tau, z)$ is of the form $P(\tau - z/c)$ where c is the speed of sound in the medium. Equation (4) can consequently be written as:

$$I_{meas}(t) = \frac{\alpha}{W}\int\int\int_{z_1}^{z_2} \sigma B_x \frac{1}{\rho c}(P(t - z/c) - P(-\infty))\, \mathrm{d}z\ \mathrm{d}x\ \mathrm{d}y, \tag{5}$$

where $P(-\infty) = 0$ since the transmitted pulse is of finite length.

Assuming B_x and c constant over space (c varies typically from −5 to +5% between soft biological tissues (Hill *et al* 2004)), and replacing the integration over z by an integration over $\tau = z/c$, equation (5) becomes:

$$I_{meas}(t) = \frac{\alpha B_x}{W}\int_{-\infty}^{\infty} H_z(\tau) P(t - \tau)\, \mathrm{d}\tau, \tag{6}$$

where $H_z(\tau) = \iint H(x', y', z' = c\tau)\mathrm{d}x'\ \mathrm{d}y'$, H is equal to $\frac{\sigma}{\rho}$ within the studied medium and 0 elsewhere. Since the medium density varies typically by a few percent between different soft tissues (Cobbold 2007), while the electrical conductivity of soft tissues can vary up to a few tens (Gabriel *et al* 1996), H can be seen mostly as a variable describing the electrical conductivity of the tissue. One can show that if the DC component of the transmitted pressure is null, then I_{meas} is null whenever the electrical conductivity is constant (Wen *et al* 1998). Thus, equation (6) shows that the measured electric current is proportional to the convolution product of a function H_z of the electrical conductivity with the axial transmitted pressure wave P.

2.3. Measured signal in B-mode ultrasound imaging

Ultrasound imaging is based on the measurement of reflections of the transmitted acoustic wave (i.e. backscattering, diffraction or specular reflection). We assume that acoustic inhomogeneities are scattering only a small part of the transmitted pressure, so that scattered waves have a negligible amplitude compared to the main acoustic beam, and that the diffraction and

attenuation are small in the region of interest. The voltage $RF\ (t)$ measured at time t on the transducer, known as the radiofrequency signal, is then equal to:

$$RF(t) = D \int_{-\infty}^{\infty} T_z(\tau) P(t-\tau)\, \mathrm{d}\tau, \tag{7}$$

where D is a constant of the transducer related to the acousto-electric transfer function, $T_z(\tau) = \iint T(x', y', z' = c\tau/2)\, \mathrm{d}x'\, \mathrm{d}y'$ with T the continuous spatial distribution of point scatterers, $P(t)$ is the axial transmitted pressure wave (the pulse shape), and $\tau = 2z/c$ (the factor 2 takes into account round-trip wave propagation in ultrasound imaging). In the latter expression of $T_z(\tau)$, the double integral is performed over a disk of diameter W (the ultrasound beam is considered as a plane wave along $\mathbf{e}_z$ inside a limited width W as in the previous section) (Bamber and Dickinson 1980). The envelope of $RF\ (t)$ represents the A-mode ultrasound signal. Note that under a more realistic incident pressure wave model, one can consider pulse beam profiles in the definition of H_z (at emission) and T_z (at emission and at reception), which can be deduced by multiplying the pulse shape with the incident pulse beam profile. Also, attenuation can be taken into account by convolution of equation (7) (and similarly, of equation (6)) with an attenuation function.

Hence, the received signal in US imaging is proportional to the convolution product of the axial spatial distribution of point scatterers T_z with the transmitted pulse shape P. If scatterers are small compared to the ultrasound wavelength, reflected waves can interfere. When the envelope of the signal is calculated and a B-mode image is formed line by line, this phenomenon appears on the image as a granular texture called acoustic speckle (Abbott and Thurstone 1979).

Apart from a proportionality coefficient, equations (6) and (7) have a similar form, where T and H play an analogous role. A speckle phenomenon is thus expected to be observed in the LFEIT technique. Its nature would be electrical, because mainly related to electrical conductivity inhomogeneities, and also acoustic, because spatial characteristics are related to the acoustic wavelength.

3. Materials and methods

Two experiments were performed in this study. The first experiment aimed at comparing a LFEIT signal and a US signal on a simple acoustic and electrical conductivity interface using the same acoustic transducer. This approach was used to perform a test with a large change in both electrical conductivity and acoustic impedance. Thus, tissue functions T_z and H_z could be considered as square pulse functions with strong gradients at the interface locations. According to the above hypotheses, the two scan line signals are expected to be identical apart from a proportionality coefficient in this special case.

The goal of the second experiment was to observe a complex biological tissue with the two imaging techniques and using the same acoustic transducer. A speckle pattern of similar spatial characteristics is expected to be observed on both types of images, since they are related to the acoustic wavelength and beam width, but different, because the nature of the imaged parameter is acoustic in one case and electrical in the other case.

3.1. Measured signal on an acousto-electrical interface

The experiment setup is illustrated in figure 2. A generator (HP33120A, Agilent, Santa Clara, CA, USA) was used to create 0.5 MHz, three cycles sinusoid bursts at a pulse repetition

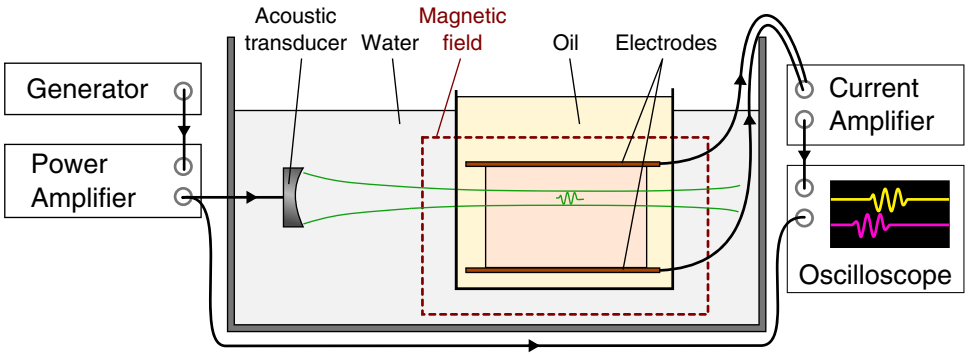

Figure 2. A transducer is transmitting ultrasound pulses toward a sample located in an oil tank placed in a magnetic field. The induced electric current is received by two electrodes in contact respectively with two sides of the gelatin.

frequency of 100 Hz. This excitation was amplified by a 200 W linear power amplifier (200 W LA200H, Kalmus Engineering, Rock Hill, SC, USA) and sent to a 0.5 MHz, 50 mm in diameter transducer focused at 210 mm and placed in a degassed water tank. The peak-to-peak pressure at the focal point was equal to 3 MPa. A $4 \times 15 \times 20$ cm^3 mineral oil tank was located from 15 to 35 cm away from the transducer in the ultrasound beam axis. This oil tank was used to decrease the loss of current from the sample to the surrounding medium and to increase consequently the signal-to-noise ratio, but was not mandatory. It was inserted in a 300 ± 50 mT magnetic field created by a U-shaped permanent magnet, composed of two poles made of two $3 \times 5 \times 5$ cm^3 NdFeB magnets (BLS Magnet, Villers la Montagne, France) separated by a distance of 4.5 cm.

The tested medium was a $5 \times 10 \times 10$ cm^3 10% gelatin filled with 5% salt sample placed inside the oil tank from 30 to 40 cm away from the transducer, and presented consequently a strong acoustic and electrical interface. A pair of $3 \times 0.1 \times 10$ cm^3 copper electrodes was placed in contact with the sample, above and under it, respectively. The electrodes were linked through an electrical wire to a 1 MV A^{-1} current amplifier (HCA-2M-1M, Laser Components, Olching, Germany). A voltage amplifier could also be used, but the current amplifier presents a smaller input impedance (a few Ohms versus 50 Ohms) and increases consequently the amount of current measured by the electrode, as depicted by the factor α in equation (4). The signals were then measured by an oscilloscope with 50 Ω input impedance (WaveSurfer 422, LeCroy, Chestnut Ridge, NY, USA) and averaged over 1000 acquisitions. US signals were simultaneously recorded using the same oscilloscope with a 1/100 voltage probe.

To quantify similarities between the two signals, we computed the correlation coefficient between them. Such coefficient is equal to 1 when the two signals are directly proportional and 0 when they are uncorrelated.

3.2. Observation of speckle in a biological tissue

The same apparatus as in the first experiment was used, but the gelatin sample was replaced by a $2 \times 6 \times 6$ cm^3 piece of bovine rib muscle purchased at a grocery store. It presented many fat inclusions, as pictured in figure 3. B-mode images were produced line by line by moving the transducer along the e_y direction by 96 steps of 0.5 mm. Acoustic and electrical signals were post-processed using the Matlab software (The MathWorks, Natick, MA, USA) by computing

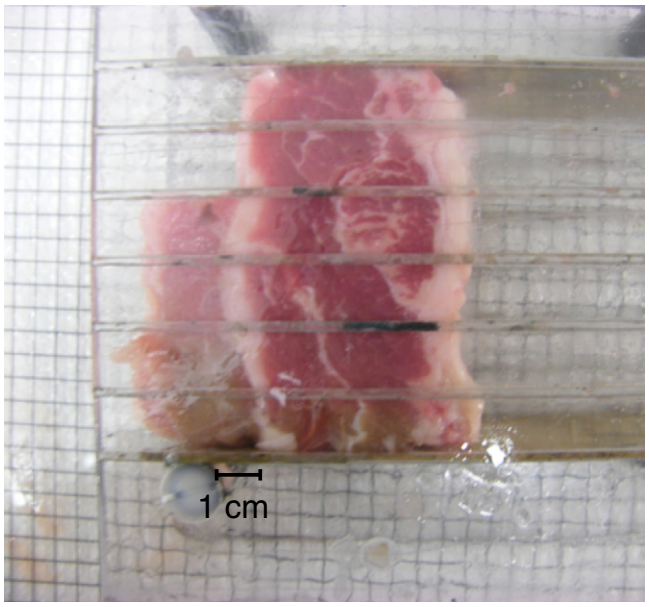

Figure 3. Picture of the $2 \times 6 \times 6$ cm^3 imaged bovine rib muscle sample, with many fat inclusions.

the magnitude of the Hilbert transform of the signal (Roden 1991), and were displayed with grayscale and jet color images, respectively.

4. Results

Figure 4(*a*) presents the electrical signal measured by electrodes from the first phantom interface, 195–220 μs after acoustic transmission, corresponding to a distance of 30 cm. Figure 4(*b*) depicts the signal acquired by the US transducer from the phantom interface, 395–420 μs after acoustic transmission, corresponding to a distance of 30 cm (back and forth). Both signals consist in three to four cycles at a central frequency of 500 kHz. The correlation coefficient between both signals is 0.9297, indicating a high similarity. This similarity was observed at the second phantom interface, with a correlation coefficient between both signals equal to 0.9179. LFEIT and US images of the phantom can be seen in Grasland-Mongrain *et al* (2013).

Figures 5(*a*) and (*b*) present the Lorentz force electrical impedance tomography image and the ultrasound image, respectively, of the bovine muscle sample. The amplitude varied from −2 to −2.8 dB with the first technique and from −1.5 to −2.5 dB with the other (0 dB being a measured amplitude of 1 V). Main interfaces of the medium can be retrieved on both images, as previously shown (Grasland-Mongrain *et al* 2013), even if signals at the boundaries and the interior of the bovine sample were of similar amplitude. A speckle pattern was present in both images. The typical spots were of size of same order of magnitude; i.e. 5–8 mm in the *Z*-direction and 10–18 mm in the *Y*-direction, but their spatial distributions were different, as expected due to the difference between the electrical and acoustic inhomogeneities. For each image, the signal-to-noise ratio was estimated as the base 10 logarithm of the ratio of the mean square amplitude of the RF signals in the 22.5–26 cm zone with the mean square amplitude in the 19–20 cm noisy zone. The signal-to-noise ratio was lower by 0.9 dB in the LFEIT image compared to the US image.

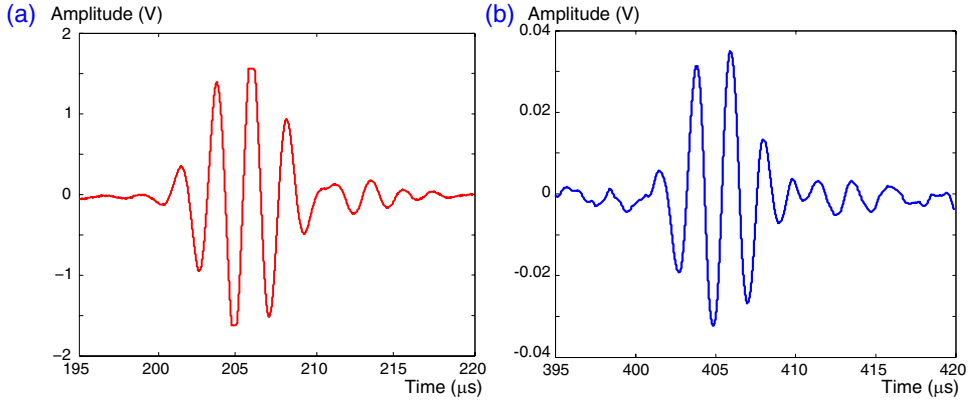

Figure 4. (*a*) Electrical signal acquired by electrodes from the first phantom interface, 195–220 μs after acoustic wave transmission. The signal is made of three to four cycles at 500 kHz. (*b*) Electrical signal acquired by the acoustic transducer from the first phantom interface, 395–420 μs after acoustic wave transmission. The signal is also made of three to four cycles at 500 kHz.

5. Discussion

The gelatin phantom used in the first experiment presented an interface of acoustic and electrical impedances. According to the correlation coefficient, the measured signals were very similar, which is a first indication of the validity of the approach presented in the theoretical section: the reflected wave is proportional to the convolution product of the acoustic impedance distribution with the transmitted ultrasound pulse shape, while the induced electric current is proportional to the convolution product of the electrical impedance distribution with the transmitted ultrasound pulse shape.

The second experiment showed two images of granular pattern. This pattern does not represent macroscopic variations of acoustic or electrical impedances, and we interpreted it as speckle. The granular pattern appeared visually with similar characteristics of size and shape in both images. Note that the size of the speckle spots along the ultrasound beam was different than in the orthogonal direction, because the first is mainly related to the acoustic wavelength and the second to the ultrasound beam width (O'Brien 1993). The spots were quite larger than those usually seen in clinical ultrasound images, due to the characteristics of the instrument (three cycles at 500 kHz, 1.5 cm beam width).

Although the bright spots were of similar size, their precise locations in the two images were different. This shows that the observed speckle reveals information of different nature in the two modalities: acoustic or electrical inhomogeneities. In this case, the bovine meat sample presented not only large layers of fat but also small inclusions of adipose tissues whose electrical conductivity differs from muscle (differences can be ten time higher at 500 kHz (Gabriel *et al* 1996)), whereas they have a close acoustic impedance (differences smaller than 10% (Cobbold 2007)).

We introduce henceforth the term ‘acousto-electrical speckle’. It is justified by the fact that its spatial characteristics are related to the acoustic parameters, especially the ultrasound wavelength, while its nature is related to the electrical impedance variation distribution H. The existence of this speckle could allow using speckle-based ultrasound techniques in the Lorentz force electrical impedance tomography technique, for example compound imaging, speckle-tracking algorithm or quantitative ultrasound for tissue characterization purposes (O'Donnell

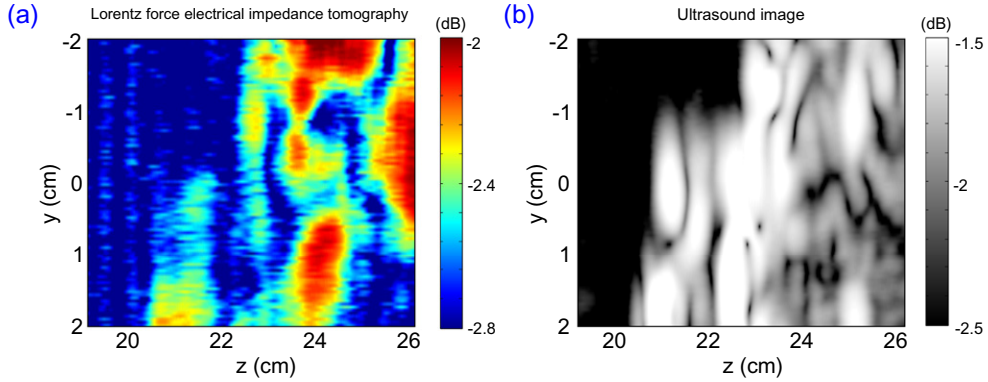

Figure 5. (*a*) Lorentz force electrical impedance tomography (LFEIT) image of the bovine muscle sample. (*b*) Ultrasound (US) image of the same bovine rib muscle sample. A speckle pattern can be seen inside the medium.

et al 1994, Jespersen *et al* 1998, Mamou and Oelze 2013). These techniques have however not be applied in this study because of the low spatial resolution of the images due to the low frequency transducer used.

This study shows that the electrical impedance inhomogeneities can be studied using LFEIT at a scale controlled by the acoustic wavelength instead of the electromagnetic wavelength, which is 5 orders of magnitude larger at a same frequency, and would be prohibitive in the context of biological tissues imaging.

These inhomogeneities should also be observed in a 'reverse' mode (terminology from Wen *et al* (1998)) called Magneto-Acoustic Tomography with Magnetic Induction, where an electrical current and a magnetic field are combined to produce ultrasound waves (Xu and He 2005, Ammari *et al* 2009, Roth 1994). However, presence of speckle in this last technique has not yet been demonstrated and which of the two methods will be most useful in biomedical imaging is not clear (Roth *et al* 2011).

6. Conclusion

In this study, the similarity between two imaging modalities, the Lorentz force electrical impedance tomography and ultrasound imaging, was assessed theoretically. This similarity was then observed experimentally on a basic acoustic and electrical interface with both methods. Then, the two techniques were used to image a biological tissue presenting many acoustic and electrical impedance inhomogeneities. The speckle pattern formed in both images exhibited similar spatial characteristics. This suggests the existence of an 'acousto-electrical speckle' with spatial characteristics driven by acoustic parameters but due to electrical impedance variation distribution. This allows considering the use of ultrasound speckle-based image processing techniques on Lorentz force electrical impedance tomography data and to study electrical inhomogeneity structures at ultrasound wavelength scale.

Acknowledgments

Part of the project was financed by a Discovery grant of the Natural Sciences and Engineering Research Council of Canada (grant # 138570-11). The first author was recipient of a

post-doctoral fellowship award by the FRM SPE20140129460 grant. The authors declare no conflict of interest in the work presented here.

References

Abbott J G and Thurstone F 1979 Acoustic speckle: theory and experimental analysis *Ultrason. Imaging* **1** 303–24

Ammari H *et al* 2009 Mathematical models and reconstruction methods in magneto-acoustic imaging *Eur. J. Appl. Math.* **20** 303–17

Ammari H, Grasland-Mongrain P, Millien P, Seppecher L and Seo J K 2014 A mathematical and numerical framework for ultrasonically-induced Lorentz force electrical impedance tomography *Journal de Mathematiques Pures et Appliquées* at press

Bamber J and Dickinson R 1980 Ultrasonic B-scanning: a computer simulation *Phys. Med. Biol.* **25** 463–79

Burckhardt C B 1978 Speckle in ultrasound b-mode scans *IEEE Trans. Sonics Ultrason.* **25** 1–6

Cobbold R S 2007 *Foundations of Biomedical Ultrasound* (Oxford: Oxford University Press)

Destrempes F and Cloutier G 2010 A critical review and uniformized representation of statistical distributions modeling the ultrasound echo envelope *Ultrasound Med. Biol.* **36** 1037–51

Destrempes F, Cloutier G 2013 Review of envelope statistics models for quantitative ultrasound imaging and tissue characterization *Quantitative Ultrasound in Soft Tissues* ed J Mamou and M L Oelze (New York: Springer) pp 219–74

Gabriel S, Lau R and Gabriel C 1996 The dielectric properties of biological tissues: II. Measurements in the frequency range 10 Hz to 20 GHz *Phys. Med. Biol.* **41** 2251–69

Goshal G, Mamou J, Oelze M L 2013 State of the art methods for estimating backscatter coefficients *Quantitative Ultrasound in Soft Tissues* ed J Mamou and M L Oelze (New York: Springer) pp 3–19

Grasland-Mongrain P, Mari J M, Chapelon J Y and Lafon C 2013 Lorentz force electrical impedance tomography *Innov. Res. Biomed. Eng.* **34** 357–60

Haider S, Hrbek A and Xu Y 2008 Magneto-acousto-electrical tomography: a potential method for imaging current density and electrical impedance *Physiol. Meas.* **29** S41–50

Hein I and O'Brien W D 1993 Current time-domain methods for assessing tissue motion by analysis from reflected ultrasound echoes—a review *IEEE Trans. Ultrason. Ferroelectr. Freq. Control* **40** 84–102

Hill C R, Bamber J C and Haar G 2004 *Physical Principles of Medical Ultrasonics* vol 2 (New York: Wiley)

Insana M F, Wagner R F, Brown D G and Hall T J 1990 Describing small-scale structure in random media using pulse-echo ultrasound *J. Acoust. Soc. Am.* **87** 179–92

Jespersen S K, Wilhjelm J E and Sillesen H 1998 Multi-angle compound imaging *Ultrason. Imaging* **20** 81–102

Lizzi F L, Greenabaum M, Feleppa E J, Elbaum M and Coleman D J 1983 Theoretical framework for spectrum analysis in ultrasonic tissue characterization *J. Acoust. Soc. Am.* **73** 1366–73

Lizzi F L, Ostromogilsky M, Feleppa E J, Rorke M C and Yaremko M M 1987 Relationship of ultrasonic spectral parameters to features of tissue microstructure *IEEE Trans. Ultrason. Ferroelectr. Freq. Control* **34** 319–29

Lubinski M A, Emelianov S Y and O'Donnell M 1999 Speckle tracking methods for ultrasonic elasticity imaging using short-time correlation *IEEE Trans. Ultrason. Ferroelectr. Freq. Control* **46** 82–96

Mamou J and Oelze M L 2013 *Quantitative Ultrasound in Soft Tissues* (New York: Springer)

Mari J M, Blu T, Matar O B, Unser M and Cachard C 2009 A bulk modulus dependent linear model for acoustical imaging *J. Acoust. Soc. Am.* **125** 2413–9

Montalibet A, Jossinet J and Matias A 2001 Scanning electric conductivity gradients with ultrasonically-induced Lorentz force *Ultrason. Imaging* **23** 117–32

Montalibet A 2002 Etude du couplage acousto-magnétique: détection des gradients de conductivité électrique en vue de la caractérisation tissulaire *PhD Thesis* Institut Nationale des Sciences Appliquées de Lyon

Noble J A and Boukerroui D 2006 Ultrasound image segmentation: a survey *IEEE Trans. Med. Imaging* **25** 987–1010

O'Brien W 1993 Single-element transducers *Radiographics* **13** 947–57

O'Donnell M, Skovoroda A R, Shapo B M and Emelianov S Y 1994 Internal displacement and strain imaging using ultrasonic speckle tracking *IEEE Trans. Ultrason. Ferroelectr. Freq. Control* **41** 314–25

Ophir J, Cespedes I, Ponnekanti H, Yazdi Y and Li X 1991 Elastography: a quantitative method for imaging the elasticity of biological tissues *Ultrason. Imaging* **13** 111–34

Roden M S 1991 *Analog and Digital Communication Systems* vol 1 (Englewood Cliffs, NJ: Prentice Hall)

Roth B J 2011 The role of magnetic forces in biology and medicine *Exp. Biol. Med.* **236** 132–7

Roth B J, Basser P J and Wikswo J P 1994 A theoretical model for magneto-acoustic imaging of bioelectric currents *IEEE Trans. Biomed. Eng.* **41** 723–8

Wagner R F, Smith S W, Sandrik J M and Lopez H 1983 Statistics of speckle in ultrasound B-scans *IEEE Trans. Sonics Ultrason.* **30** 156–63

Wen H, Shah J and Balaban R S 1998 Hall effect imaging *IEEE Trans. Biomed. Eng.* **45** 119–24

Xu Y and He B 2005 Magnetoacoustic tomography with magnetic induction (MAT-MI) *Phys. Med. Biol.* **50** 5175–92

Yamaguchi T 2013 The quantitative ultrasound diagnosis of liver fibrosis using statistical analysis of the echo envelope *Quantitative Ultrasound in Soft Tissues* ed J Mamou and M L Oelze (New York: Springer) pp 275–88